491

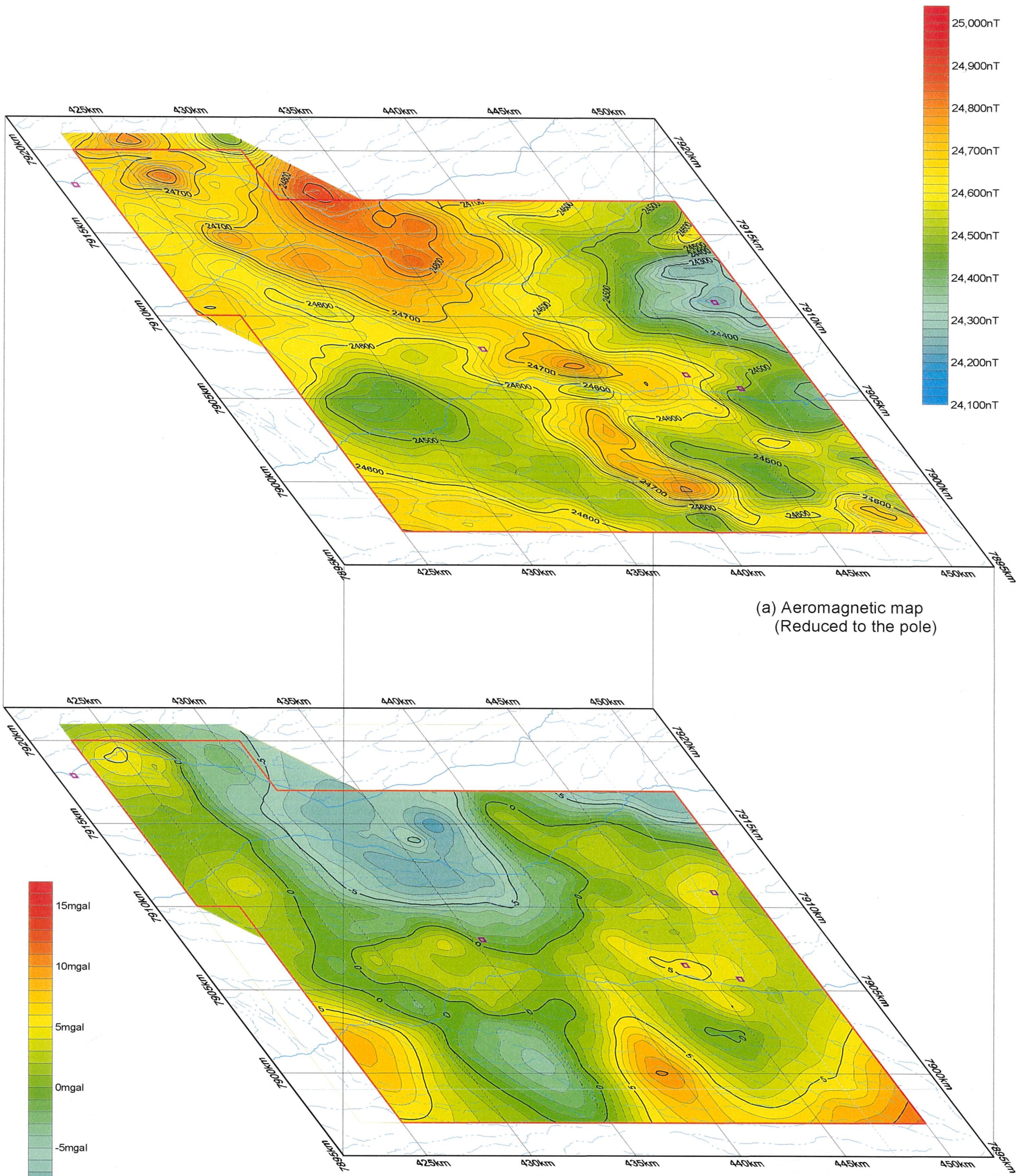

(a) Aeromagnetic map
(Reduced to the pole)

(b) Gravity anomaly map
(First order residual)

Fig. 2-3-6 Panel Diagram of Aeromagnetic Map and Gravity Map

basement (thickness of the volcanic rocks) by the following process. The subsurface density structure is divided into the upper and lower layers with the basement surface as the boundary, and then the density contrast ($\Delta \rho$) of the two layers are varied. Modeling was carried out for three density contrasts; $\Delta \rho = 0.30$, 0.40, and 0.50g/cm^3. Assuming the average density of the basement to be 2.65g/cm^3, the average density of the upper layers will be 2.35, 2.25, and 2.15g/cm^3.

The control points for two-layer modeling were set at locations where the basement is exposed at the surface for profiles A-A' and B-B'. Since the basement is not exposed along the C-C' profile, the calculated depth of A-A' profile at the intersection between C-C' and A-A' profiles was used as the control point.

The stratigraphic division used for multi-layer modeling is as follows.

Quaternary System	
Conglomerate・gravel layer	2.00g/cm^3
Agglomerate/andesite・basalt	2.25/2.60g/cm^3
Neogene System	
Low-density ignimbrite (mainly pumiceous tuff)	1.85g/cm^3
High-density ignimbrite (mainly welded tuff)	2.30g/cm^3
Conglomerate	2.15g/cm^3
Basement complex	
(Upper Cretaceous, Upper Cretaceous・Paleogene Systems, intrusive rocks)	
Rhyolitic pyroclastics, andesite lava, andesite pyroclastics	2.65g/cm^3
Diorite porphyry	2.67g/cm^3
Quartz diorite	2.65g/cm^3
Quartz porphyry・granodiorite	2.55g/cm^3

Density value of 2.25g/cm^3 was used for Quaternary agglomerate・andesite・basalt in localities with higher occurrence of agglomerate, and 2.60g/cm^3 for localities with higher andesite and basalt occurrence. Density data regarding conglomerate and gravel layers are lacking, and the value 2.00g/cm^3 was determined by trial and error method seeking fair agreement of calculated and measured gravity anomaly values.

The Neogene ignimbrite was divided into two groups, low-density and high-density groups. This division is based on average density of naturally dried values. High-density ignimbrites constitute the major part of the upper layer in two-layer modeling, and 2.25g/cm^3

was considered to be the appropriate density from the modeling results. Thus the actual density of the high-density ignimbrite is most probably lower than the average density 2.33g/cm^3 of rock samples and the value 2.30g/cm^3 was used. There are no density data regarding conglomerate. And since conglomerate is somewhat denser than agglomerate and less dense than ignimbrite, we arrived at the value of 2.15g/cm^3 for density of conglomerate.

Regarding the density of the basement complex, 2.65g/cm^3 was used because Upper Cretaceous andesitic lava and pyroclastics are the main component. For quartz diorite of the intrusive bodies, 2.65g/cm^3 of the Upper Cretaceous System was used. At first, calculation was carried out using 2.65g/cm^3 for diorite porphyry (A-A' profile), but the calculated gravity anomaly did not agree with the measured values and finally 2.67g/cm^3 was decided to be the appropriate value. The measured density of quartz porphyry and granodiorite samples is about 2.50g/cm^3. But measured and calculated gravity anomalies of the Quebrada Camarones of B-B' profile and the southern bank of the Quebrada Camerones in A-A' profile do not agree unless extremely small bodies are assumed or higher density is used. Thus density values higher than the measured values were used.

(1) A-A' profile

This is a profile that joins the northwestern part of the survey area and the southeastern part. High gravity anomaly occurs on both ends and low anomaly in the central part of this profile. Basement complex is exposed in a very narrow zone of the Quebrada Vitor in the northwest and near Esquiña and on the southern bank of Quebrada Camarones in the eastern part. Control point for two-layer modeling was set at the diorite porphyry exposure near Esquiña.

The basement surface by two-layer analysis is close to the surface near Quebrada Vitor in the northwest with all density contrasts and agrees well with the actual geology. On the other hand, on the southern bank of the Quebrada Camarones where basement is exposed, the calculated basement does not reach the surface and does not agree with the actual geology. The following two reasons are considered to cause this discrepancy.

① There are no stations on the southern bank of the Quebrada Camarnes where this profile passes through, and thus the gravity anomaly does not accurately reflect the geology.

② The basement complex on the southern bank of the Camrones has lower density compared to that of the basement near Esquiña where the control point is set.

Regarding ②, high-density diorite porphyry and diorite actually occur near Esquiña and relatively loiw-density granodiorite occurs on the southern bank of the Camarones.

The thickness of the upper layer in this profile is maximum near the intersection with C-C' profile and reaches 1,600m at $\Delta \rho$ =0.30g/cm^3 (2.35/2.65g/cm^3), 1,000m at $\Delta \rho$ =0.50g/cm^3 (2.15/2.65g/cm^3). It is difficult to determine the appropriate density contrast for this profile, but for the nest B-B' profile $\Delta \rho$ =0.40g/cm^3 appears to be the most appropriate density contrast.

The relief of the basement surface by multi-layer modeling is close to the results of two-layer modeling by $\Delta \rho$ =0.40g/cm^3. The basement surface gradually lowers toward the central part of the profile from the uplifted parts in the northwest and along the drainage basin of the Quebrada Camarones. The elevation of the deepest part is calculated to be about 1,500m above sea level. The difference of elevation between the uplifted arts in the northwest and along the Quebrada Camarones and the lowest part is 500~700m.

Intrusive bodies (quartz diorite, diorite porphyry, and granodiorite) were assumed at three localities from geological data, at northwestern part, Esquiña, and southern bank of the Quebrada Camarones. As quartz diorite has the same density as the Upper Cretaceous System in the vicinity, the gravity anomalies are calculated to be the same regardless of the shape of the bodies. Therefore, it is noted that the shape of the quartz diorite bodies in the figure was not important during the modeling.

Although only one quartz diorite body is shown at the uplifted art in northwest, magnetic anomaly profile shows two magnetic anomalies and there is a possibility of another quartz diorite intrusion on the northwestern side of the present intrusive body. Also magnetic anomaly profile shows the coincidence of high magnetic anomaly and diorite porphyry occurrence near Esquiña and of low magnetic anomaly and granodiorite occurrence on the southern bank of the Quebrada Camarones.

Regarding the relation between gravity anomalies and magnetic anomalies, extremely high correlation is observed between low gravity anomaly and high magnetic anomaly in the central part of the profile and between high gravity anomaly and low magnetic anomaly in the southeastern part of the profile.

(2) B-B' profile

This is a profile joining the northwestern part and southern part of the survey area. High gravity anomalies occur at both ends of the profile and low gravity anomaly occurs on the northwestern side of the central part and small high gravity anomaly on the southeastern side. Basement complex outcrops occur at three localities; near the Quebrada Vitor in the northwest at the intersection with the A-A' profile, in the Quebrada Camarones zone in the central part, and in the southernmost part of the area. Of the above three exposures, control point for two-layer modeling was fixed at the granodiorite outcrop in the southernmost part where the gravity anomaly is the highest.

The basement surface by two-layer modeling is near the surface for all three-density contrasts near the Qubrada Vitor in the northwest and coincides well with the geology. On the other hand, the result of the modeling differs by the density contrast in the Quebrada Camarones zone. The basement surface is deepest at 200~400m below the surface with $\Delta \rho = 0.30 g/cm^3$, and greatly differs from the actual geology. With $\Delta \rho = 0.40 g/cm^3$, although the basement complex reaches the surface at the Quebrada Camarones, it does not reach the surface at the middle slope of the southern bank of the Quebrada Camarones where the basement complex actually is exposed. With $\Delta \rho = 0.50 g/cm^3$, the basement reaches the surface extensively close to the actual distribution of the basement complex from the south bank to the north bank of the Quebrada Camarones, but the measured and calculated gravity anomaly values do not agree in some parts.

From the above, the selection of the most probable basement surface would first eliminate the results of $\Delta \rho = 0.30 g/cm^3$. Comparing the results of the remaining $\Delta \rho = 0.40 g/cm^3$ and $\Delta \rho = 0.50 g/cm^3$, agreement with actual geologic occurrences is better with $\Delta \rho = 0.50 g/cm^3$, but $\Delta \rho = 0.40 g/cm^3$ is more appropriate with the density of the upper layer. Density contrast of $\Delta \rho = 0.50 g/cm^3$ would correspond to the average density of the upper layer of $2.15 g/cm^3$, which is far below the range of inferred density, 2.23~$2.35 g/cm^3$ and is much too low. On the other hand, $\Delta \rho = 0.40 g/cm^3$ corresponds to the average density of $2.25 g/cm^3$ for the upper layer which is within reasonable range. Thus this figure is considered to be best suited for use in two-layer modeling.

The thickness of the upper layer along this profile attains maximum value near the intersection with C-C' profile and attains 1,000m with $\Delta \rho = 0.40 g/cm^3$, 1,450m with $\Delta \rho = 0.30 g/cm^3$, and 750m with $\Delta \rho = 0.50 g/cm^3$. On the southern bank of the Quebrada Camarones, the thickest part of the upper layer is calculated to be 600~700m ($\Delta \rho = 0.40 g/cm^3$).

The relief of the basement surface by multi-layer modeling is close to the result of two-layer modeling with $\Delta \rho = 0.40 g/cm^3$. The basement surface which is largely uplifted at the southernmost part of the survey area gently drops toward the northwest, and after the lowest point near the intersection with C-C' profile, gradually rises to the northwest. The elevation of the lowest part near the intersection with C-C' profile is about 1600m above sea level and the difference of elevation between the highest point in the southernmost part reaches 1,200m. Although it is not known accurately because of erosion and landslides, the basement was possibly uplifted locally near the Quebrada Camarones.

In this profile, intrusive bodies (quartz diorite, quartz porphyry, and quartz diorite) are assumed, in accordance with geological data, at three localities, namely the northwestern part, the northern bank of the Quebrada Camarones, and the southernmost part of the area. The quartz diorite bodies at both ends of the profile do not have density contrast with the rocks of the vicinity as in the case of A-A' profile, and thus the shape of the figure is not the result of modeling.

A small low gravity anomaly occurs at the central part of a local high gravity anomaly extending on both banks of the Quebrada Camarones. This low gravity coincides with high local magnetic anomaly and corresponds with the occurrence of quartz porphyry. Quartz porphyry has lower density compared to the basement rocks in the vicinity and is appropriate to be expressed as a local low gravity. But if we assume a density of $2.50 g/cm^3$ for the quartz porphyry, the intrusive body will have to be extremely small for the calculated and measured gravity anomalies to coincide. The shape of the body in the figure is drawn by assuming $2.55 g/cm^3$ density, but the calculated and measured values do not approximate sufficiently. For the two values to approximate closely, either the intrusive body should be small or use density value closer to $2.65 g/cm^3$. But since two-dimensional assumption does not describe the body sufficiently, agreement of details would not be appropriate. It is also possible that the small size of the intrusive body indicates that the profile passes through the peripheral parts of the rock. Residual map of Figure 2-3-4 indicates eastward expansion of the local low gravity anomaly, and the center of the quartz porphyry body may be located to the east of the profile.

High correlation is observed between low gravity anomalies and high magnetic anomalies on the northwestern side of the central part of the magnetic anomaly profile. This is similar to A-A' profile. The high gravity anomalies at both ends of the profile do not coincide with low

A - A'

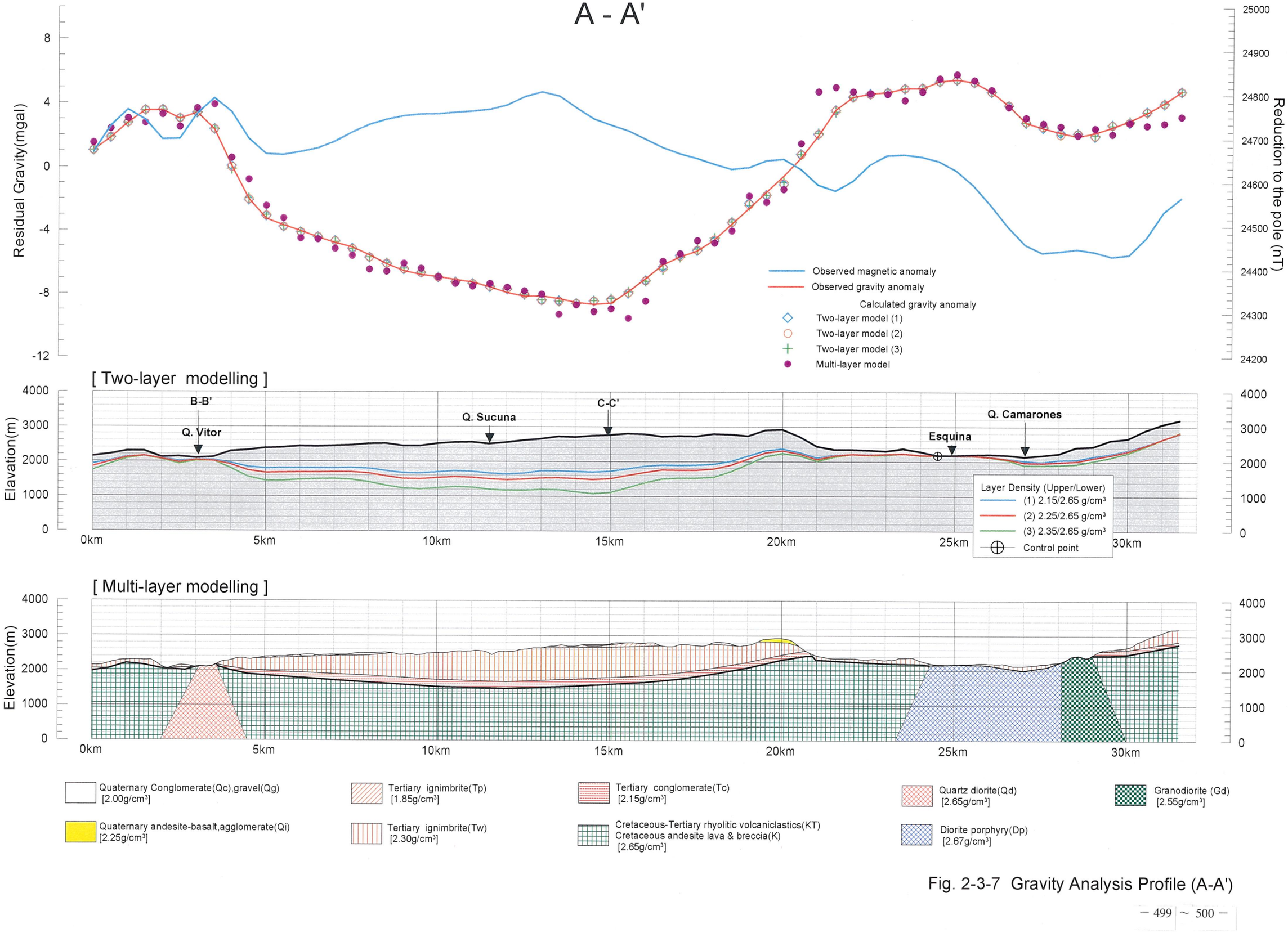

Fig. 2-3-7 Gravity Analysis Profile (A-A')

B - B'

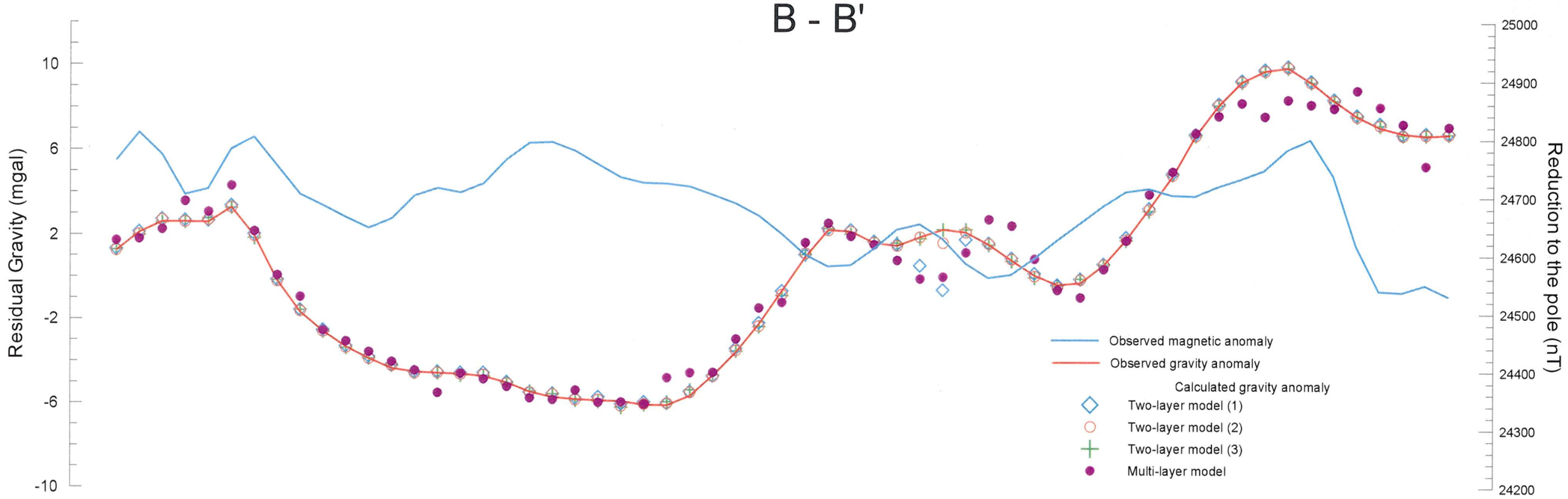

[Two-layer modelling]

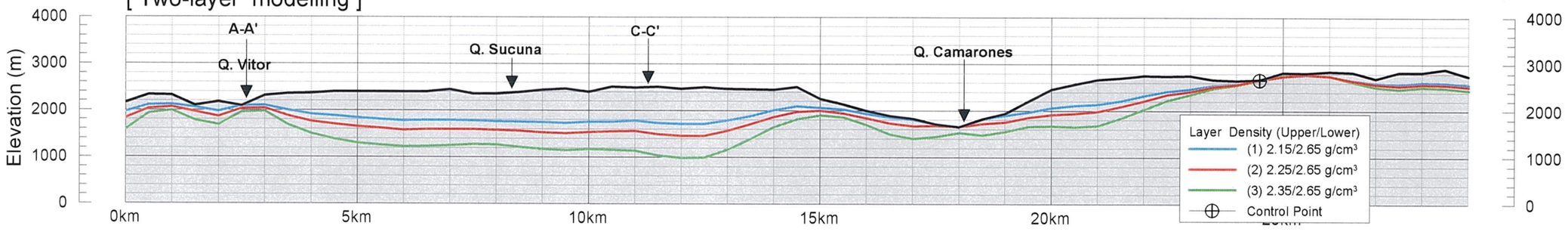

[Multi-layer modelling]

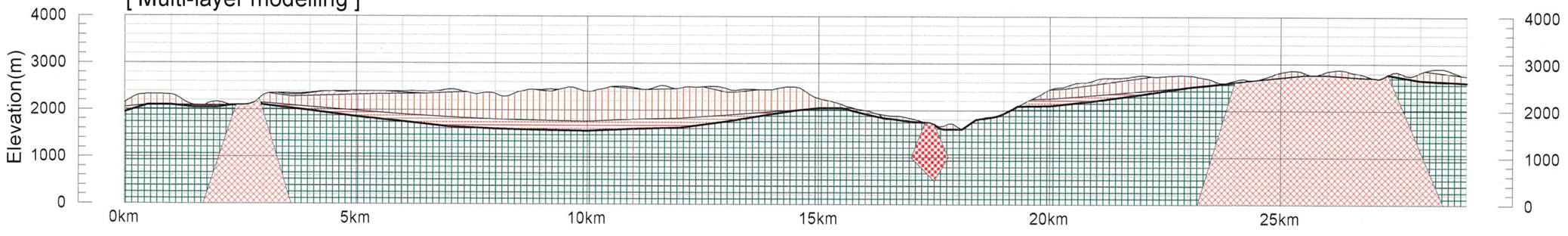

Quaternary Conglomerate(Qc),gravel(Qg) [2.00g/cm³]

Tertiary ignimbrite(Tw) [2.30g/cm³]

Cretaceous-Tertiary rhyolitic volcaniclastics(KT)
Cretaceous andesite lava & breccia(K) [2.65g/cm³]

Quartz porphyry(Qp) [2.55g/cm³]

Tertiary ignimbrite(Tp) [1.85g/cm³]

Tertiary conglomerate(Tc) [2.15g/cm³]

Quartz diorite(Qd) [2.65g/cm³]

Fig. 2-3-8 Gravity Analysis Profile (B-B')

C - C'

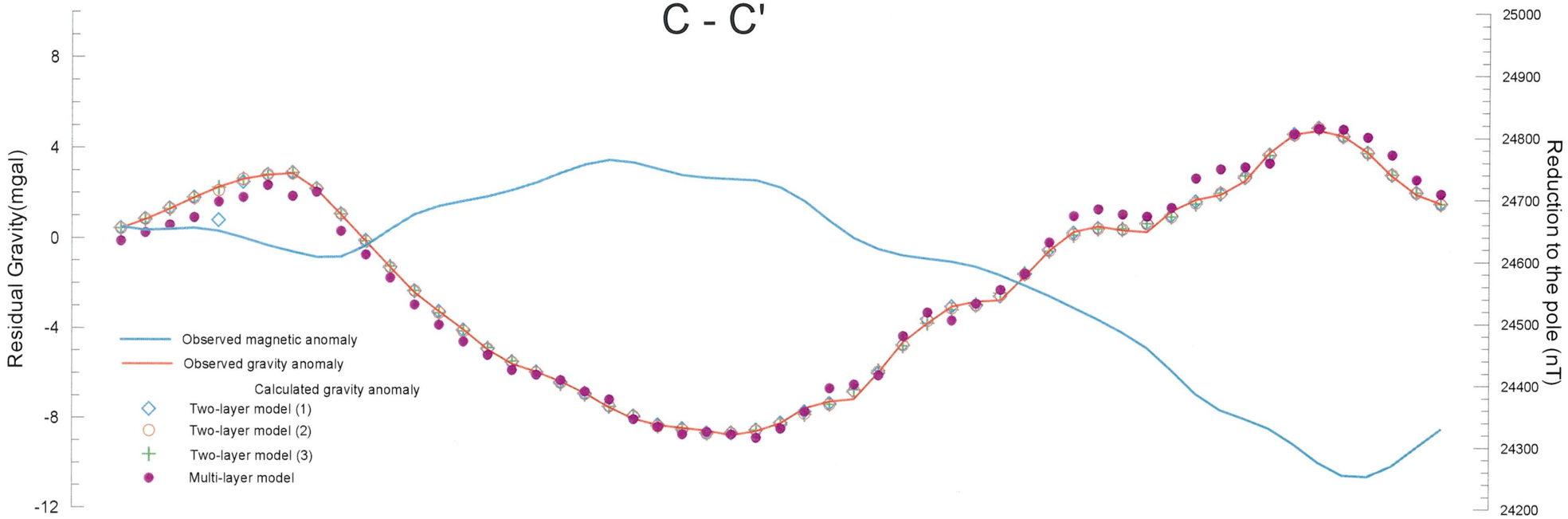

[Two-layer modelling]

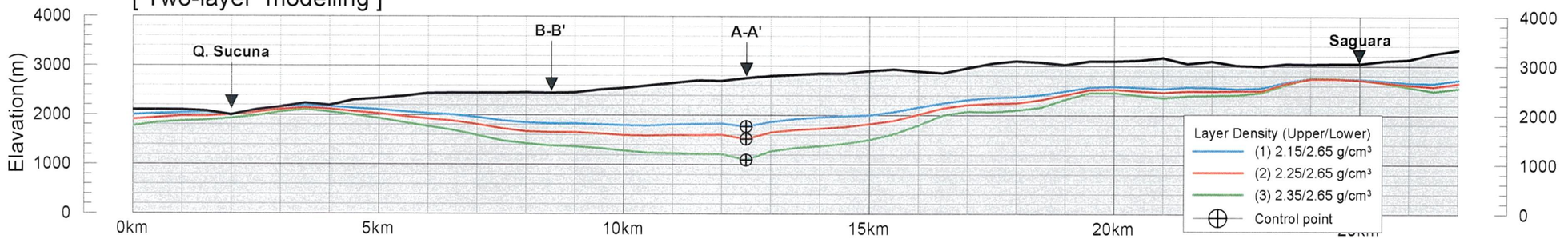

[Multi-layer modelling]

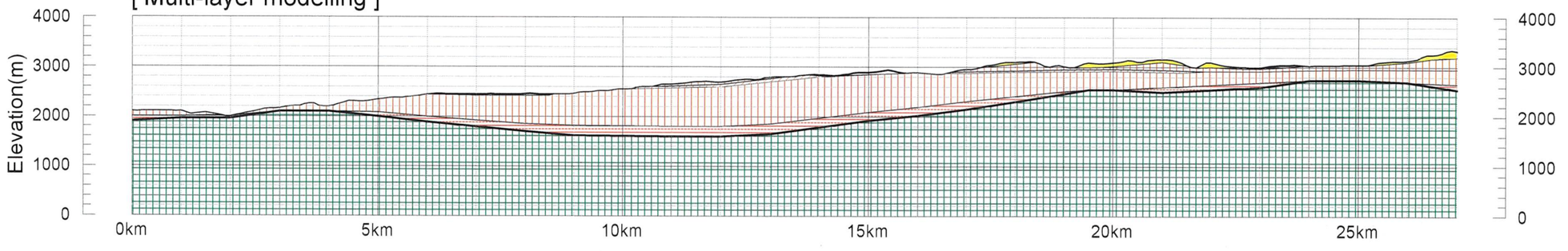

Quaternary Conglomerate(Qc),gravel(Qg) [2.00g/cm³]

Quaternary andesite-basalt(Qi) [2.60g/cm³]

Tertiary ignimbrite(Tp) [1.85g/cm³]

Tertiary ignimbrite(Tw) [2.30g/cm³]

Tertiary conglomerate(Tc) [2.15g/cm³]

Cretaceous-Tertiary rhyolitic volcaniclastics(KT)
Cretaceous andesite lava & breccia(K) [2.65g/cm³]

Fig. 2-3-9 Gravity Analysis Profile (C-C')

magnetic anomalies and this is interpreted to be the effect of the high magnetic anomalies corresponding to the intrusive body.

(3) C-C' profile

This is a profile joining the western part and the eastern part of the survey area. High gravity anomalies occur at both ends and low gravity anomaly in the central part. Basement rocks are not exposed along the profile.

The basement surface by two-layer modeling is close to the surface at the high gravity anomaly zone in the west regardless of the density assumed. Lowest Neogene conglomerate is confirmed in the vicinity and the result is harmonious with the actual geologic occurrences. On the other hand, shallowest depth of about 300m is calculated for the basement surface in the high gravity anomaly zone in the east near Saguara. The upper layer is thickest near the intersection with A-A' profile and it is calculated to be about 1,200m with $\Delta \rho = 0.40 g/cm^3$.

The basement surface relief by multi-layer modeling is similar to the calculated results of two-layer modeling with $\Delta \rho = 0.40 g/cm^3$. The basement surface is shallow in the western part of the profile, but the scale of uplifting is larger in the eastern part, and the difference of elevation of the surface in the eastern uplifted part and the central sunken part is 1,100m.

3-2-5 Three-dimensional analysis

Three-dimensional two-layer modeling was carried out in order to clarify the relief of the basement surface and the thickness of the overlying volcanic rocks. The density contrast between the basement rocks and the upper layers (volcanic rocks) was assumed to be $\Delta \rho = 0.40 g/cm^3$, and the control point was fixed in the basement exposure (diorite) near Esquiña.

(1) Relief of the basement surface

The results of three-dimensional two-layer modeling with $\Delta \rho = 0.40 g/cm^3$ are shown in Figure 2-3-10. The contours indicate the elevation of the basement surface.

Figure 2-3-10 shows that the basement surface of the survey area is relatively high in the southeastern and eastern part and is low along the Quebrada Camarones. Some of the southeasternmost and easternmost parts are more than 3,000m above sea level and further rises to the southeast. The basement surface drops steeply for about 400m, during a short

distance of 2km from 442km to 440km in UTM coordinates to the north of the Quebrada Camarones, large relief exceeding 300m do not occur to the west of this zone. The lowest basement surface aside from the Quebrada Camarones is in the zone from middle stream of Quebrada Sucuna to middle Quebrada Vitor, and in the lower reaches of Quebrada Sucuna, and the elevation is calculated to be 1,700~1,800m.

Comparison of the results of the three-dimensional two-layer modeling and two-dimensional two-layer modeling shows that the three-dimensional modeling results in 100~200m higher at the basement drop in middle Sucuna, about 100m higher near Saguwara in the east, and 300m lower in the high gravity anomaly zone in the southernmost part of the area.

(2) Thickness of the upper layers (volcanic rocks)

Figure 2-3-11 shows the values obtained by subtracting the elevation of the upper surface of the basement laid out in Figure 2-3-10 from the elevation of the surface, namely the thickness of the upper layer overlying the basement. The upper layer contains conglomerate at the bottom, but most of it is composed of ignimbrite.

It is seen from Figure 2-3-11 that either the upper layer is less than 100m thick or the basement is exposed at; along the Quebrada Camarones, the downstream part of the Quebrada Vitor, near Suguwara in the eastern part, southeastern margin, and other parts of the area. This agrees with actual distribution of the basement rocks in the drainage zone of the Quebrada Camarones, with the exception of the downstream part, and the lower reaches of the Quebrada Vitor. The occurrence of the basement complex is not confirmed in the southeasternmost part of the survey area, but an extensive high gravity anomaly is observed in the southeastern part, and thus the possibility of the occurrence of basement rocks in the shallow subsurface zones is high.

The upper layer is thicker than 500m at; an extensive zone from middle stream of the Quebrada Sucuna to the middle to upstream part of Quebrada Sucuna, and a belt on the southern bank of the upper stream to middle stream of Quebrada Camarones. There are localities with the upper layer reaching a thickness over 1,000m from the northern to the northeasternmost parts with high elevation and in the southeastern part of the area.

3-2-5 Discussions

The results of gravity survey are summarized in figure 2-3-12. In this figure important

factors for future exploration in this area are shown. They are; thickness of the upper layer (mainly ignimbrite), elevation of the upper surface of the basement, outline of the gravity distribution, and the extension of intrusive bodies inferred from gravity and magnetic data.

(1) Gravity anomalies and geology

The basement complex of this area occurs extensively from the middle stream to upstream of the Quebrada Camarones, and small exposures are also confirmed in the lower stream of the Quebrada Vitor in the northwesternmost part and in the southernmost part. Localities of basement complex occurrence all show high gravity anomalies and close relation between the basement complex and high gravity anomaly has been confirmed. Measurements of rock samples show that the basement rocks have density 0.40g/cm^3 higher than that of the ignimbrite which extensively cover these rocks. Thus the density of the rocks backs the relation between the basement rocks and high gravity anomaly.

The density structure of this area can be basically approximated by two-layer structure, the upper volcanic layer consisting mainly of ignimbrite and the lower basement complex. From the above relation between the high gravity anomaly and the basement rocks, it is inferred that the high gravity anomalies occur where the basement complex is either exposed on the surface or in shallow subsurface zones, namely ignimbrite is either thin or lacking. And low gravity anomalies occur where the basement is relatively deep, namely ignimbrite is thick. Figure 2-3-12 shows that the zone with 300~500m-thick upper layer is the boundary between the high and low gravity anomaly zones.

Cretaceous to Tertiary intrusive bodies are included in the basement complex. Quartz diorite and diorite porphyry, however, have density very close to that of the Upper Cretaceous System which constitutes the main part of the basement. Therefore it is difficult to extract the existence of these two rock types or to consider their subsurface extension by gravity data alone. Quartz porphyry and granodiorite have density 0.10~0.15g/cm^3 lower than the Upper Cretaceous System and may cause local low gravity anomaly within high anomaly zones. Diorite, on the other hand, has higher density and may cause local high gravity anomaly. However, local anomalies within high gravity anomaly zones could be caused by lower-density ignimbrite or basalt on the surface and the cause can only be determined by correlation with the surface geology. Also many of the intrusive rocks have relatively high magnetism, and the use of magnetic anomaly maps would increase the reliability of interpretation.

(2) Gravity anomalies and magnetic anomalies

It was pointed out in section 3-2-2 that "high gravity – low magnetism" and "low gravity – high magnetism" relation holds for relatively extensive anomalies, and that "high gravity – high magnetism" and "low gravity – low magnetism" relation holds for anomalies of local scale. The "low gravity – high magnetism" relation is observed most clearly in the low gravity anomaly between the middle stream of the Quebrada Sucuna and the middle stream of the Quebrada Vitor. Thick ignimbrite is inferred to occur in this zone from gravity analysis and the high magnetic anomaly is believed to be caused by this ignimbrite. Generally welded tuff does not have high magnetism, but magnetite content affects the magnetism and this ignimbrite is considered to have high magnetite content.

"High gravity – low magnetism" is typically observed in the eastern part of the survey area where the basement complex is believed to occur in shallow subsurface zones. Upper Cretaceous andesitic rocks generally have high magnetism, but that of the eastern part of this area clearly correspond to low magnetic anomaly. Therefore the Cretaceous System of this area is believed to have low magnetism. The reason for this low magnetism could be; ① magnetism of the Upper Cretaceous rocks is lower than that of ignimbrite, ② the Upper Cretaceous rocks lost their magnetism for some reason, ③ the remnant magnetism of the Upper Cretaceous units is reverse.

"High gravity – high magnetism" is observed in local anomalies at northwest margin of the area, east of Pachica in the central part, near Esquiña, and southern to southernmost part. Intrusive bodies occur in all of the above zones such as; quartz diorite in the northwesternmost and the southern~southernmost parts, quartz porphyry at east of Pachica, and diorite porphyry near Esquiña, and these are considered to be the cause of the anomalies.

"Low gravity – low magnetism" is observed at two localities, southeastern part at the southern bank of the Quebrada Camarones and southern~southwestern part of the area. The results of gravity analysis (Fig. 2-3-11) indicate the possibility of ignimbrite deposition with thickness of 500~1,000m in these localities. This fact negates the "ignimbrite=high magnetism" mentioned earlier, and indicates the existence of ignimbrite with low magnetism. It is possible that magnetism of ignimbrites varies by sedimentary units, but data on Camarones district alone is insufficient and this needs to be investigated on a larger scale.

(3) Basement structure inferred from the results of gravity analysis

Rise of the basement is seen, in Figure 2-3-10, at two localities, one in the eastern and the other in the southeast to southernmost parts of the area. These two topographic highs are located to the north and south of the Quebrada Camarones and these are considered to have had been a single rise which was subsequently dissected by the Quebrada Camarones. Reconstruction of pre-erosion basement would result in an extensive topographic high exceeding 2,500m in elevation in the eastern ~southeastern~southern part of the survey area. This basement rises steeply in the southeast direction and drops gently in the W~NW direction. This is a monotonous drop in the westerly direction to about 2,000m above sea level. Then further westward the basement is almost horizontal with relatively low relief in the order of 200m and elevation of around 2,000m. This topography extends in the north to northwest to western part of the survey area. In parts where the basement is lower than 2,000m in elevation, ignimbrite thicker than 500m is probably distributed extensively.

It is noted that the basement surface of Figure 2-3-10 has many steep slopes between 2,300 and 2,700m elevation. If these slopes are the products of erosion, it most probably reflects the difference of lithology of the basement. On the other hand, if this is the product of uplift, the steep slopes may reflect the boundary of blocks.

(4) Distribution of intrusive bodies inferred from gravity and magnetic anomalies

Local distribution of high magnetic anomalies is shown in Figure 2-3-12. Of the magnetic anomalies, those corresponding to local high gravity anomalies are; two at the northwestern margin of the area, two in the southern part, and one near Esquiña. Regarding the four magnetic anomalies, excluding the one on the northern side of the northwestern margin, the one on the southern side of the northwestern margin and the two in the southern part correspond to quartz diorite intrusive bodies and the anomaly near Esquiña to diorite porphyry. At the two magnetic anomalies in the northwestern margin, the high gravity anomaly indicates the existence of one large intrusive body. This is a good possibility, and even if there are two bodies, the magnetic anomalies have common features and their depth of occurrence and magnetism are similar.

A magnetic anomaly corresponding to a local low gravity anomaly within or near a high gravity anomaly occurs to the east of Pachica in the central part of the area. The low gravity anomaly in this case is a saddle of a high gravity anomaly zone and is not a notable one. Quartz porphyry occurs to the west of the magnetic anomaly and the extension of the magnetic anomaly most probably represents the subsurface distribution of the intrusive body. The density of the quartz porphyry is lower than other rocks of the basement complex, and

the above agrees also with the local low gravity anomaly.

Local high magnetic anomalies not associated with gravity anomalies occur at five localities from the northern to the northwestern part of the area. These magnetic anomalies are located in a zone of thick ignimbrite distribution and it cannot represent intrusive bodies in shallow subsurface zones. These anomalies possibly represent the variation of magnetic properties of ignimbrite.

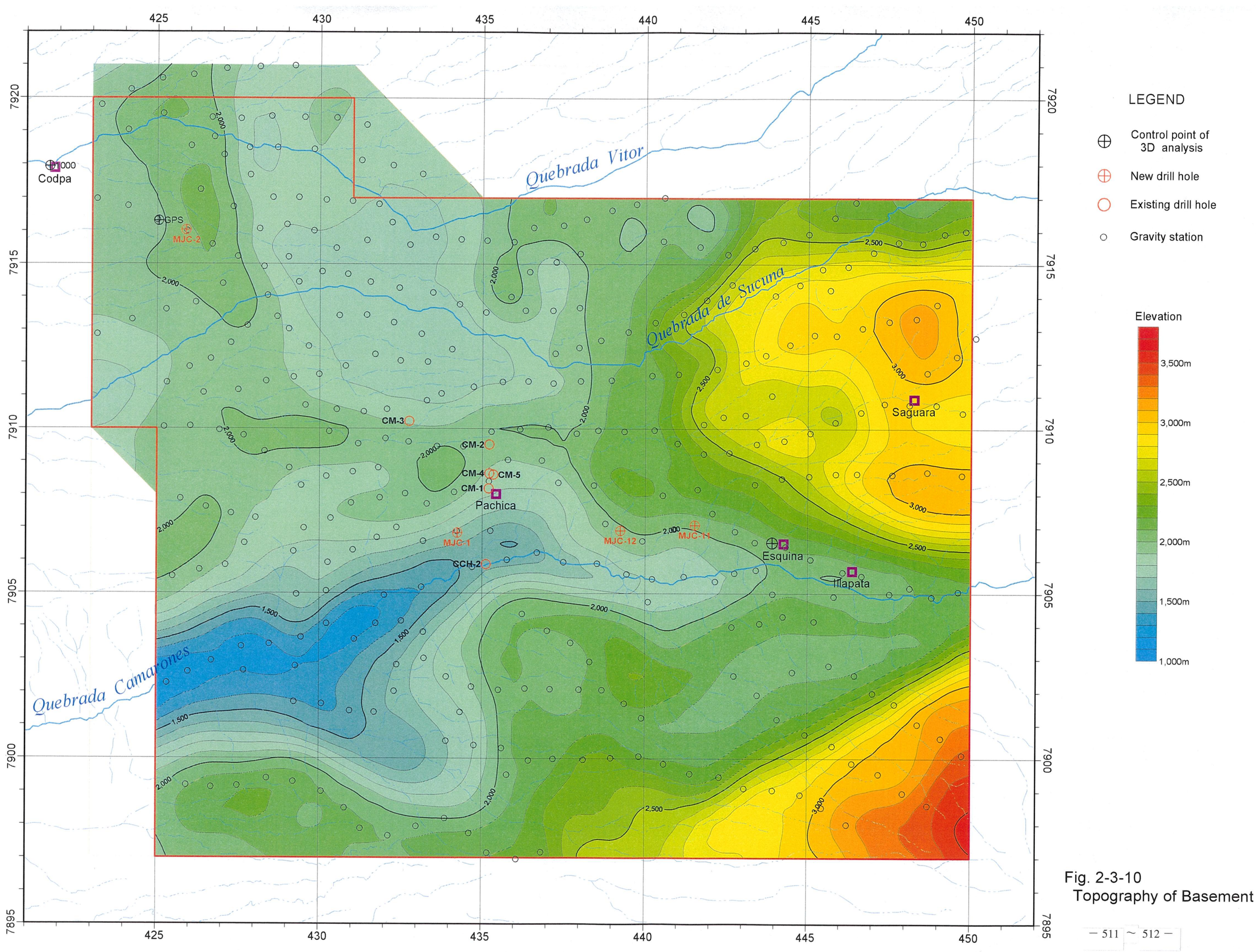

Fig. 2-3-10
Topography of Basement

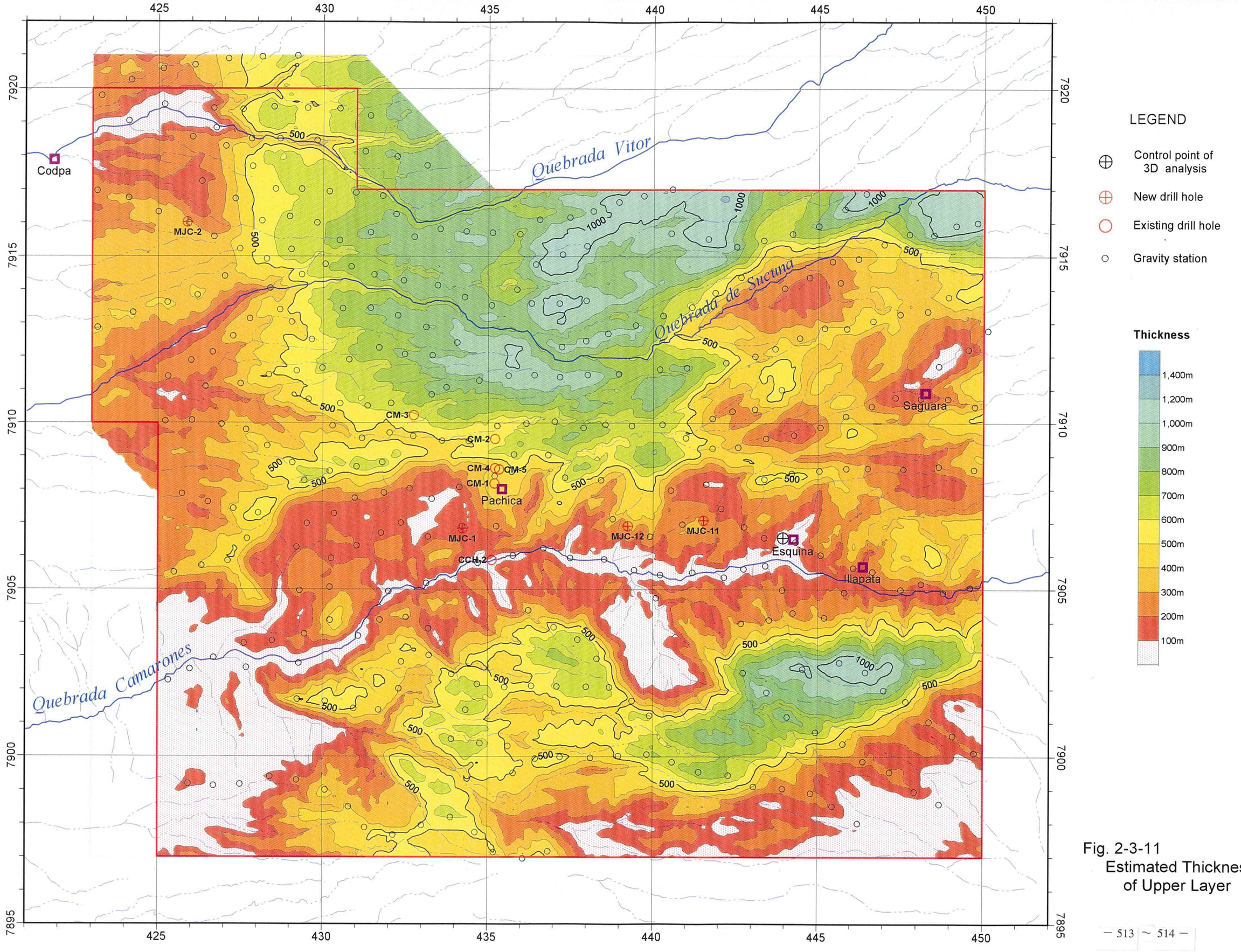

Fig. 2-3-11
Estimated Thickness of Upper Layer

LEGEND

- Gravity high
- Gravity low
- High gravity gradient zone
- Local magnetic high correspond to local gravity high
- Local magnetic high correspond to local gravity low
- Local magnetic high
- New drill hole
- Existing drill hole
- Gravity station
- Topography of basement

Thickness of upper layer

- 1,400m
- 1,200m
- 1,000m
- 900m
- 800m
- 700m
- 600m
- 500m
- 400m
- 300m
- 200m
- 100m

Fig. 2-3-12
Gravity Interpretation Map

CHAPTER 4 AIRBORNE MAGNETIC SURVEY

4 - 1 Survey methods

4-1-1 Field work

(1) Project area

The survey area is shown in Figure 2-3-1. Airborne magnetic data for subareas A and B were newly flown and acquired, data for C was purchased from Fugro Airborne Survey Pty (FAS), and those for D were supplied by CODELCO. Analysis was carried out for all A ~D. Data for C and D were compiled.

(2) Aircraft and base airports

A fixed wing twin engine aircraft (Registration No. C-GGVR) was used for the survey. Specifications are for standard models modified for airborne magnetic survey.

The base airports were Iquique for the southern part of the survey and Alica for the northern part of the survey.

(3) Survey specifications

FAS acquired data for the North Chile Survey using the following parameters. Flight line direction N-S, flight line spacing 500m, tie line spacing 5,000m, tie line direction 90 degrees, total length including tie lines 31,100km.

Sensor height was 100m nominal subject to discretion of the pilot.

(4) Equipment

The following major equipment were used during the airborne data acquisition.

- Magnetometer: CS-2 optically pumped cesium magnetometer
- Navigation equipment: No1Ael 12 channel high speed GPS receiver
- Data acquisition system: Minmag data acquisition

(5) Data acquisition

The following digital data were recorded in magnetic disk. The quality of the acquired data was subsequently checked to see that they satisfied the specifications.

a. Flight time
b. Radar altitude

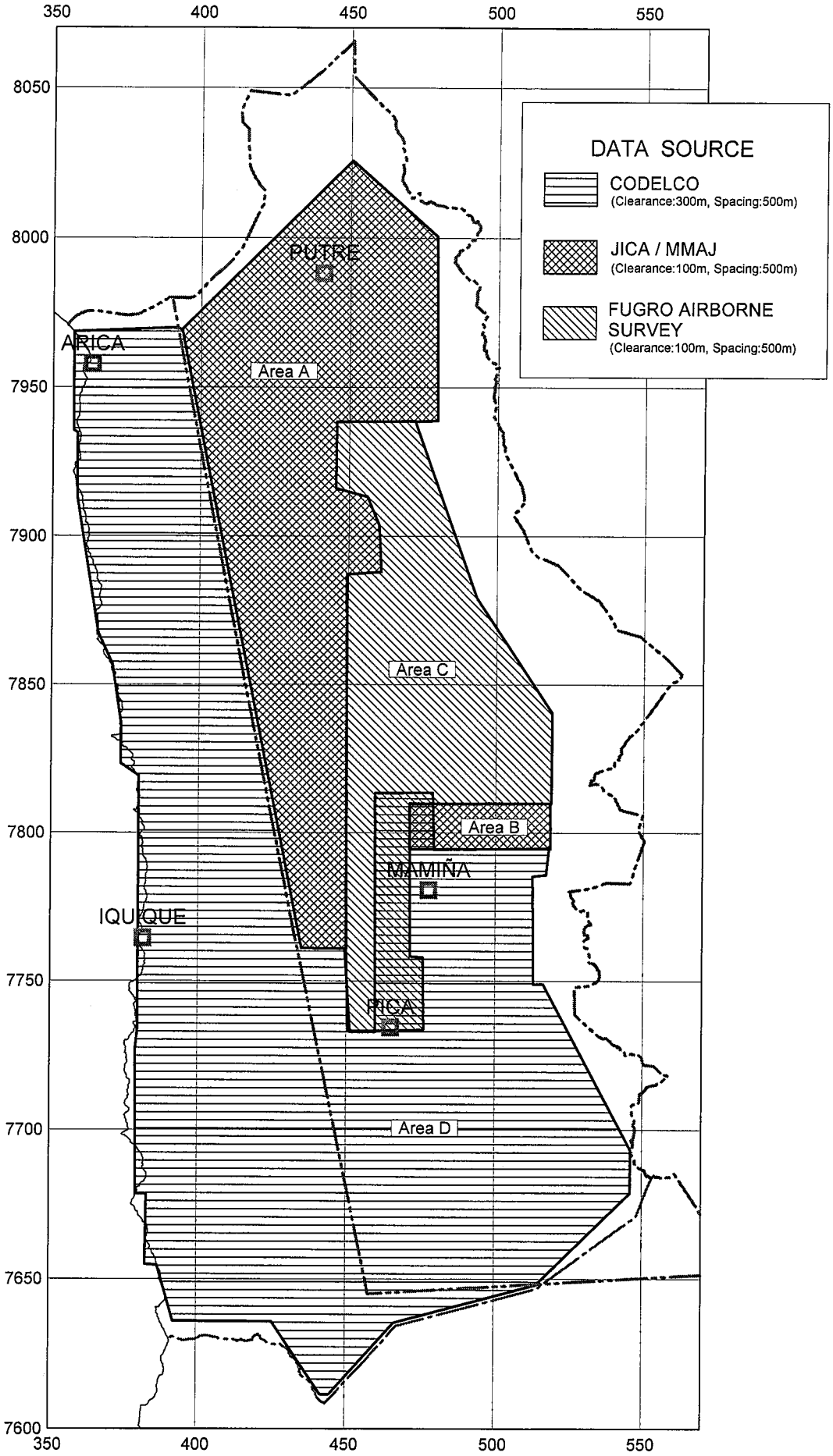

Fig.2-4-1 Survey Area of Airborne Magnetic Survey

c. Barometric altitude
d. Magnetometer readings (before compensation)
e. Magnetometer readings (after compensation)
f. GPS readings
g. Develco 3 axes fluxgate magnetometer information
h. Manually inserted information such as flight number and line number.

The resolution of the magnetometer and the GPS data sampling interval were as follows.

a. Magnetometer cycle rate 0.1 seconds
b. Magnetometer resolution 0.001nT
c. GPS cycle rate 1 second

(6) Ground magnetometer

Diurnal magnetic variations and magnetic storm activity were measured with a Gem GS-19 Overhauser proton precession magnetometer or alternative cesium magnetometer. Output was digitally recorded on a PC computer that also recorded GPS time to a precision of 0.005 seconds for synchronization of airborne and ground magnetic data.

The instrument had a resolution of 0.01nT, a noise envelope of better than +/−0.1 nT and digital output was provided and recorded once every 2 seconds or less. Longer sampling times reduced the noise envelope.

The base station magnetic monitors (cesium optical pumping magnetometer) were located at about 10km north of Iquique airport and at near the Alica airport.

4-1-2 Data processing

1) The acquired data were checked for noise level and flight path, and then sent to the Fugro office in Perth. There magnetic diurnal variation, level, and other relevant processing was made. They were converted to gridded data and the following magnetic maps and images were prepared. Maps were projected in Universal Transverse Mercator (UTM) Zone 19 using WGS 84 datum. Maps were plotted at an appropriate scale, showing UTM and graticular coordinates and were produced on the HP650c Designjet plotter using a stable Mylar base or paper.
   - Final flight path map
   - Final color contour map TMI/RTP
   - Final color TMI/1VD image

- Final greyscale TMI/1DV image
- Stacked profiles of TMI
- Final colored DTM (digital terrain model) image

Final gridded and located digital data were provided in ER Mapper/Surfer/format on CD-ROM consisting of:

- Corrected TMI
- Corrected TMI/RTP
- Corrected TMI/1VD

The raw data were supplied on CD-ROM as located data in ASCII format containing the following information. Line number, flight number, date, time, fiducial number, UTM coordinates, total magnetic intensity value, magnetic diurnal value, IGRF, radar altimeter reading, barometric altimeter reading, GPS, Digital terrain.

4-1-3 Interpretation

The magnetic data were qualitatively analyzed using a methodology based on that outlined by Isles et al. (2000), and Nash & Rankin (1994). This is typically a multi-stage (and multi-level) process involving:

a. Extraction of the position of shallow magnetic units.

b. Extraction of magnetic trend and distribution caused by rock distribution, alteration, and relevant factors.

c. Extraction of deeper concealed magnetic rock bodies or structures from lower frequency magnetic signals. The position and shape of such bodies are generally more subjective than those of shallow zones, as resolution of magnetic sources decreases with increasing distance between source and sensor.

d. Geologic contacts, fault/shears are compiled by recognition of changes in magnetic character or texture between differing units or domains. And angular discordance, breaks or inflexions between and along major magnetic units. Both major and minor faults/shears are interpreted from:

- overall distribution of magnetic trends and units
- direct observation of magnetic anomalies associated with the structure and
- profile modeling of magnetic signals.

The resulting structural framework was compared with GIS data set of the published geological maps and also with JICA/MMAJ Landsat interpretation (JICA, 2000). Although the majority of structure interpreted from the magnetic data was found to have a high degree

of correlation with the published mapping, several differences were apparent in differing zones:

a. Some faults mapped on the surface were not evident in the data.
b. Faults mapped at the surface were close to but not coincident with faults interpreted from the magnetic data.
c. Faults interpreted from the magnetic data were not recorded in zones of outcrops in the published maps.

Many of the faults recorded in the published maps appear as late-stage normal faults cross-cutting the overall N-S structure grain of the region. Where these have only minor movement, or occur in magnetically quiet regions, their expression in the magnetic data is generally ambiguous. N-S trending structural elements are commonly difficult to detect in the magnetic data, as they parallel the flight lines of the magnetic surveys. This problem has also been noted in other regional interpretations of magnetic data-sets within the Andean belt (eg. Chernikoff et al., 1996, Rankin & Triggs, 1997).

Resolution of structures parallel to the flight line direction increases with closer line spacing. Numerous structures recorded within the published maps were integrated with magnetic interpretation.

・Detailed interpretation of the Camarones district

Detailed structural interpretation was carried out for the Camarones district shown in the following figure 2-3-2.

・Two-dimensional modeling of target profiles

Three promising target zones have been profiled using two-dimensional modeling. The target zones are two profiles in the Camarones district and one in the Escondida district.

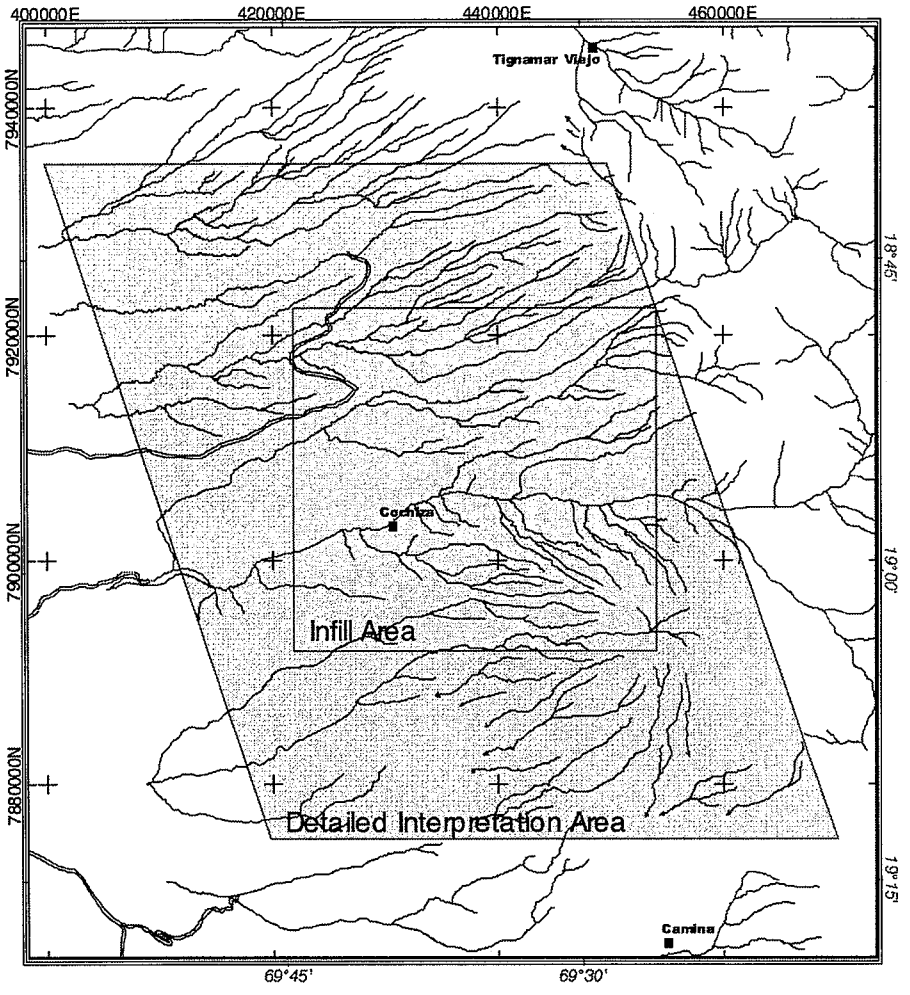

Fig. 2-4-2. Location of the detailed 1:100 000 'solid geology' interpretation area

4 - 2 Results of survey

Interpretation of airborne magnetic data from the Northern Chile Region I has focussed on providing:

a. a structural view of the regional geologic framework for the Andean Belt;
b. a detailed geological interpretation of a key target area (Camarones district) by the Metal Mining Agency of Japan;
c. a quantitative geophysical analysis of depth to basement and 2-dimensional modeling of selected target profiles.

The magnetic data was a combined stitch of existing multiclient data (supplied by Fugro Airborne Surveys), and proprietary data (supplied by CODELCO), plus newly acquired data.

4-2-1 Regional structural framework

This interpretation emphasizes the primary underlying structural features controlling distribution of the various litho-tectonic suites throughout the region, and their role in focussing both magnetic and mineralizing events (at the expense of detailed interpretation of surficial or near surface lithologies).

The tectonic overview highlights the subdivision of the region into several subdomains: a regional migration of magmatic activity can be traced east to west. The western Cretaceous La Negra / Coastal Batholith magmatic arc was superseded by the interpreted Paleocene Tarapaca Back Arc magmatic belt. Further east, the deformed Mesozoic sediment / volcanic sequences and eastern Paleozoic basement were intrud3ed by early-middle Tertiary intrusives (porphyry-related). These were superseded by a weakly-discordant series of Mid-Tertiary to Recent volcanic centers trending NNW. The main Early Tertiary intrusive complexes also follow a NNW discordant structural trend.

The various subdomains define a roughly N-S regional grain for the Andean Belt, with a significant bend towards the NNW north of ~20° S (coincident with Tertiary-Quaternary magmatism).

Several major NE, NE, and E-W transfer fault zones or corridors are highlighted in the regioal structure. These have been active during several deformational episodes, and have played a major role in focusing both mineralized porphyry and epithermal systems within this region, and throughout the rest of the Andean Belt.

The northern continuation of several crustal-scale orogen - parallel fault systems associated with major mineralization throughout Central and Northern Chile have been interpreted from the magnetic data, including the Domeyko Fault System (DFS). This structure is related to the western fault margin of Paleozoic basement, and is the regional structural locus for the giant copper porphyries at Escondida, El Salvador, Chuquicamata, Collahuasi, Quebrada Blanca, and others.

A series of subvolcanic intrusive and caldera structures have also been interpreted from the data. Many of these are coincident with both known mineralization and regional structures.

A series of target zones have been selected for both porphyry copper and epithermal / volcanic dome related Au/Ag mineralization. These targets are based on associations of confluence of regional structures, localized and regional magnetic characteristics, and

distribution of known mineralization.

The most prospective exploration districts occur within four significant zones, spaced approximately 80km apart, along a subtle NNW trending structural corridor (these include the districts hosting Collahuasi and Cerro Colorado).

4-2-2 Detailed solid geology interpretation

A detailed solid geology interpretation, emphasizing the local relationships of near-surface lithology to the regional structure and underpinning intrusives, has been completed over a specified area of approximately 60km×60km. This area covers one of the four significant exploration districts mentioned above. Two main target zones have been identified, within which are contained several discrete magnetic anomalies for follow-up work.

4-2-3 Two dimensional modeling of target profiles

Three of the most promising target zones have been profiled using two-dimensional geophysical modeling. The first two profiles cover the perceived best magnetic anomaly from each of the two primary target zones identified in the detailed solid geology interpretation. The third, identified in the regional structural interpretation, has been positioned over a zone exhibiting similar overall tectonic and magnetic features to that of the Escondida area.

4-2-4 Depth to magnetic source analysis map

A regional study has been undertaken across the entire North Chilean airborne magnetic data set, to determine the depth to the source of significant tectonic structures. The technique used to determine depths in this study was the Werner method. Final solutions have been presented as both spot depths and gradient contours.

The depth solutions derived from the Werner process were shown to fall into three fairly distinct regions which coincided well with the regional tectonic framework. The deeper solutions (>800m) are shown to concentrate in the middle of the data set, within the Trapaca Back Arc Magmatic Belt. A slightly shallower group (600~800m) corresponding to the Coastal Batholith tectonic subdomains, lie to the west of the Tarapaca Belt. On the east side of the data set, beyond the interpreted extension of the Domeyko Fault System, the depth solution rise to an average of 400m. This corresponds to the Paleozoic basement subdomains identified in the regional interpretation.

CHAPTER 5 DRILLING SURVEY

5-1 Objectives, Drilling Sites, and Geologic boundaries

Twelve holes were drilled in order to clarify the geology and alteration associated with mineralization in zones where the intermediate airborne magnetic intensity zones and the peripheries of the medium wavelength anomalies overlap.

The drill site, collar elevation, and the location of main geologic boundaries are shown in Table 2-5-1.

5-2 Geology, Mineralization and Alteration of the Drill Holes

Geologic columns of the drill holes, results of X-ray diffraction, results of thin section study of representative samples, and the results of polished section examination of ore samples are appended at the end of this volume. Also the results of chemical assay are laid out in Table 2-5-2, Figure 2-5-4, and in the Appendix.

The results of the investigation of the drill holes are reported below, from north southward.

(1) East Arica area (MJC-8)

A geological map of the area is shown in Figure 2-2-90 and a geological cross section in Figure 2-2-91.

① Geology

The geology of this hole consists of, from bottom upward, Oligocene-Miocene conglomerate, Miocene-Pliocene ignimbrite, and alluvial gravel.

The conglomerate is pale green, and contains propylitic andesite, granitic rocks, porphyry, and quartzite rounded gravel, and the lower part frequently contains intercalation of thin layers of pale green tuffaceous sandstone.

The ignimbrite is gray to brown, and consists of quartz, biotite, plagioclase and minor rock fragment-bearing rhyolitic welded tuff.

The gravel bed consists of pumiceous tuff, propylitic andesite, and granitic gravel.

Table 2-5-1 Location of Holes and Geologic Boundaries

MJC-1

COORDINATES		Dip angle (°)
Northing	Easting	
7906836	434234	-90
Hole depth (m)	Elevation (m)	GEOLOGIC BOUNDARY
0	1825.0	
136	1689.0	Tig / Kgd
144	1681.0	Kgd / Kv(i)
348	1477.0	Bottom of Hole

MJC-2

COORDINATES		Dip angle (°)
Northing	Easting	
7916018	425878	-90
Hole depth (m)	Elevation (m)	GEOLOGIC BOUNDARY
0	2410.0	
82	2328.0	Qcp / Tig
318	2092.0	Tig / Tc
500	1910.0	Bottom of Hole

MJC-3

COORDINATES		Dip angle (°)
Northing	Easting	
7923936	428041	-90
Hole depth (m)	Elevation (m)	GEOLOGIC BOUNDARY
0	2509.0	
342	2167.0	Tig / Tc
500	2009.0	Bottom of Hole

MJC-4

COORDINATES		Dip angle (°)
Northing	Easting	
7933518	434372	-90
Hole depth (m)	Elevation (m)	GEOLOGIC BOUNDARY
0	3126.0	Tig
500	2626.0	Bottom of Hole

MJC-5

COORDINATES		Dip angle (°)
Northing	Easting	
7937942	443117	-90
Hole depth (m)	Elevation (m)	GEOLOGIC BOUNDARY
0	3567.0	
14	3553.0	Qvc / Tig
500	3067.0	Bottom of Hole

MJC-6

COORDINATES		Dip angle (°)
Northing	Easting	
7941669	445282	-90
Hole depth (m)	Elevation (m)	GEOLOGIC BOUNDARY
0	3541.0	
368	3173.0	Qvc / Qv
402	3139.0	Bottom of Hole

MJC-7

COORDINATES		Dip angle (°)
Northing	Easting	
7936453	453301	-90
Hole depth (m)	Elevation (m)	GEOLOGIC BOUNDARY
0	3809.0	
212	3597.0	Qvc / Qv
382	3427.0	Bottom of Hole

MJC-8

COORDINATES		Dip angle (°)
Northing	Easting	
7956731	409060	-90
Hole depth (m)	Elevation (m)	GEOLOGIC BOUNDARY
0	1911.0	
54	1857.0	Qal / Tig
276	1635.0	Tig / Tc
500	1411.0	Bottom of Hole

MJC-9

COORDINATES		Dip angle (°)
Northing	Easting	
7879115	428742	-90
Hole depth (m)	Elevation (m)	GEOLOGIC BOUNDARY
0	1672.0	
66	1606.0	Qcp / Qvr
174	1498.0	Qvr / TQc
500	1172.0	Bottom of Hole

MJC-10

COORDINATES		Dip angle (°)
Northing	Easting	
7883670	472132	-90
Hole depth (m)	Elevation (m)	GEOLOGIC BOUNDARY
0	3802.0	
6	3796.0	Qal / Qv
394	3408.0	Bottom of Hole

MJC-11

COORDINATES		Dip angle (°)
Northing	Easting	
7907077	441528	-90
Hole depth (m)	Elevation (m)	GEOLOGIC BOUNDARY
0	2334.0	
138	2196.0	Tig / Tc
428	1906.0	Tc / Kgd
498	1836.0	Kgd / Tgd
500	1834.0	Bottom of Hole

MJC-12

COORDINATES		Dip angle (°)
Northing	Easting	
7906907	439245	-90
Hole depth (m)	Elevation (m)	GEOLOGIC BOUNDARY
0	2292.0	
18	2274.0	Qal / Tig (talus)
32	2260.0	Tig (talus) / Qcp
66	2226.0	Qcp / Tig
116	2176.0	Tig / Tc
300	1992.0	Bottom of Hole

abbrev. : Qal=alluvial (gravel), Qcp=colluvial (gravel, talus), Qvc=Quaternary conglomerate-sandstone
Qv=Quaternary-Tertiary andesite-basalt with tuff, Qvr=Quaternary-Tertiary rhyolitic ignimbrite, TQc=Quaternary-Tertiary conglomerate with pumice tuff
Tig=Pliocene-Miocene rhyolitic ignimbrite
Tc=Miocene-Oligocene conglomerate with tufaceous sandstone
Tgd=Tertiary intrusive rock (diorite porphyry, quartz diorite)
Kgd=Cretaceous-Tertiary intrusive rock (quartz porphyry)

② Alteration-mineralization

Neither alteration nor mineralization is observed in this hole.

(2) Area to the northwest of Tignamar (MJC-4,5,6,7)

A geological map of the area is shown in Figure 2-2-75 and a geological cross section in Figure 2-2-76.

MJC-4:

① Geology

The geology of this hole consists of ignimbrite.

The ignimbrite of this hole is brown, and is composed of quartz-biotite-bearing rhyolitic welded tuff and the lower part contains intercalation of thin dark gray conglomerate layers consisting of andesite pebbles.

② Alteration-mineralization

Neither notable alteration nor mineralization are observed in this hole, only existence of quartz veinlets is inferred at 476~482m depth interval.

MJC-5:

① Geology

The geology of this hole consists of Miocene-Pliocene ignimbrite, with occurrence of Upper Neogene-Quaternary felsic pumiceous tuff at the surface.

The ignimbrite is gray~brown, and consists of rhyolitic welded tuff containing quartz, biotite, plagioclase, and minor amount of rock fragments.

The pumiceous tuff is white with minor amount of rock fragments.

② Alteration-mineralization

Notable alteration-mineralization is not observed in this hole, but epidote have been identified microscopically in weakly silicified part at 340m depth. Also limonite dissemination is recognized at 158~160m and 178~186m depth intervals. Alunite was identified from 158m depth sample. The results of chemical analysis of the above alteration zone indicated high As anomaly (Table 2-5-2).

MJC-6:

① Geology

The geology of this hole consists of Upper Neogene-Quaternary gravel layer, with intercalation of siltstone and pumiceous tuff. Also basalt occurs at the lower part of the hole.

The gravel layer is gray and consists of andesite~dacite pebbles. The pebble size varies considerably and changes from fine pebble layer, through coarse sand layer to silt layer.

The pumiceous tuff is white and dacitic.

Basalt is dark gray and is ferromagnetic.

② Alteration-mineralization

Notable alteration-mineralization is not observed, but yellow altered part occurs in pumiceous tuff at 90~92m and 100~102m depth intervals, and reddish alteration occurs in gravel layer at 124~128m depth interval and in pumiceous tuff at 134~146m depth interval. Sericite and jarosite were identified in 124m depth sample. High As anomaly in the above alteration zone was confirmed by chemical analysis (Table 2-5-2).

MJC-7:

① Geology

The geology of this hole consists of, from bottom upward, Upper Neogene-Quaternary basalt, mafic andesite・mafic andesitic pyroclastic rocks and gravel layer.

The basalt and mafic andesite are both black and form alternation with intercalation of pyroclastic rocks.

Gravel bed is brown to gray and consists of andesite~dacite and silicified rhyolite pebbles.

② Alteration-mineralization

Notable alteration nor mineralization occur in this hole, but there are; reddish altered parts in the gravel layer at 78~80m, 98~100m, 132~134m, and 166~170m depth intervals. Also there is a yellow alteration part in andesite at 248~250m depth interval. Sericite and kaolin were identified from sample at 168m depth. Relatively high As anomaly was detected from alteration zones at 78~80m and 98~100m depth intervals (Table 2-5-2).

(3) Codpa area (MJC-2, 3)

A geological map of the area is shown in Figure 2-2-73, and geological section in Figure 2-2-74.

MJC-2:

① Geology

The geology of this hole consists of, from bottom upward, Oligocene-Miocene conglomerate, Miocene-Pliocene ignimbrite, and Pleistocene and Holocene gravel bed.

The Oligocene-Miocene conglomerate has intercalation of pumiceous tuff and tuffaceous sandstone in the lower part.

The ignimbrite is brown and consists of quartz-biotite-bearing rhyolitic welded tuff.

The Pleistocene-Holocene gravel contains large amount of ignimbrite pebbles.

② Alteration-mineralization

Neither alteration nor mineralization is observed in this hole.

MJC-3:

① Geology

The geology of this hole consists of, from bottom upward, Oligocene-Miocene conglomerate, Miocene-Pliocene ignimbrite and Pleistocene-Holocene gravel.

The Oligocene-Miocene conglomerate has intercalation of thin dacitic pumiceous tuff in the lower part.

The ignimbrite is brown and consists of quartz-biotite-bearing rhyolitic welded tuff.

The Pleistocene Holocene gravel consists of andesite and pumiceous tuff pebble.

② Alteration-mineralization

Neither alteration nor mineralization is observed in this hole.

(4) Camarones area (MJC-1, 11, 12)

A geological map of the area is shown in Figure 2-5-2 and geological cross section in Figure 2-5-3.

MJC-1:

① Geology

The geology of this hole consists of Upper Cretaceous andesite, Upper Cretaceous-Paleogene quartz porphyritic breccia and Miocene-Pliocene ignimbrite.

The andesite is strongly sericitized and chloritized, but porphyritic texture is observed.

The quartz porphyritic breccia is sericitized with cataclastic texture and is oxidized to reddish brown.

The ignimbrite is purplish gray to brown and consists of quartz-biotite-bearing rhyolitic welded tuff. Conglomerate below the ignimbrite is lacking in this hole, and thus this ignimbrite is inferred to be a landslide deposit.

② Alteration-mineralization

The quartz porphyritic breccia and andesite below 136m depth have been sericitized and silicified and is accompanied by chloritization below 185m depth.

The quartz porphyritic breccia has been strongly limonitized in 136~142m depth interval and this is an oxidized zone. Also relatively strong pyrite dissemination occurs in the quartz porphyritic breccia and andesite below 142m depth. Copper minerals could not be identified by unaided eyes in this hole. Copper content is somewhat larger below 306m compared to the upper part (Fig. 2-5-4).

MJC-11

① Geology

The geology of this hole consists of, from bottom upward, Upper Cretaceous-Paleogene diorite porphyry・quartz porphyry, Miocene conglomerate and Miocene-Pliocene ignimbrite.

The diorite porphyry is dark gray, and is sericitized and chloritized and accompanied by pyrite dissemination.

Quartz porphyry is white to gray and contains large quartz phenocrysts (3-5mm).

The conglomerate consists of quartz diorite, quartz porphyry, granodiorite, andesite, silicified

rock, tuffaceous sandstone pebbles, and contains intercalation of thin white to pink volcanic ash layers.

The ignimbrite is red to purplish gray and consists of quart-biotite-bearing welded tuff.

② Alteration-mineralization
Quartz porphyry and diorite porphyry are strongly sericitized and silicified below 428m depth.

The quartz porphyry below 456m depth is oxidized and is limonitized, and relatively strong pyrite dissemination is observed in quartz porphyry and diorite porphyry below 456m depth. It was not possible to identify copper minerals by unaided eyes in this hole. Also the assay indicated low grade (Fig. 2-5-4).

MJC-12:
① Geology
The geology of this hole consists of Upper Cretaceous-Paleogene quartz diorite, Miocene conglomerate, Miocene-Pliocene ignimbrite, and Quaternary gravel.

The quartz diorite is dark green, and is chloritized and epidotized.

The conglomerate contains quartz diorite pebbles, and intercalation of thin silt~sandstone layers and pumiceous tuff layers.

The ignimbrite is reddish brown, and consists of dacitic pumiceous tuff and quartz·biotite -bearing rhyolitic welded tuff.

The Quaternary gravel layer contains intercalation of ignimbrite, but it is considered to be a landslide deposit.

② Alteration-mineralization
Quartz diorite below 164m depth is relatively strongly propylitized and partly sericitized with weak pyrite dissemination.

Copper minerals could not be identified by unaided eyes, but assay indicated relatively high Cu background value (Fig. 2-5-4).